

## FINAL SCIENTIFIC REPORT

**PROJECT TITLE:** The influence of maternal bonding in neuroimmune synaptic sculpting

**YEAR:** 2019

**APPLICATION ID:** A-10860

**PRINCIPAL INVESTIGATOR:** Ana Luísa Colaço Cardoso

### 1. BRIEF INTRODUCTION AND WORK HYPOTHESIS:

The bond between a mother and her child, which is established in early life, has a profound longitudinal impact in the child's development and mental health and is highly susceptible to the influence of environmental stressors. Exposure to early-life stress (ELS), such as that caused by maternal separation or neglect (physical, emotional and cognitive), can induce maladaptive behaviors and increase vulnerability to neurological disorders later in life<sup>1</sup>, leading to an annual estimated cost of \$500 billion in US alone. Although ELS has been recognized as one of the most relevant risk factors for a range of psychiatric disorders and medical conditions, the rate of several of these disorders, including schizophrenia, autism spectrum disorders and depression, differ significantly between males and females, raising the important but still unanswered question of whether sex modulates the consequences of ELS<sup>2</sup>.

In rodents, like in humans, the peri-natal period is a critical time window for the establishment and maturation specific neuronal circuits and long-range connections. Sexual dimorphic variations also emerge during this period, due to a surge of testosterone in males, which is aromatized and locally converted to estrogens, leading to several structural and functional differences between the male and female brain. These differences are maintained and accentuated by the different levels of sexual hormones that start to be produced during adolescence, after the onset of reproductive age (i.e. testosterone in males and estrogens and progesterone in females). This intrinsic variability in brain connectivity and sex hormone levels has been pinpointed as a potential explanation to the different responses males and females present to stress, injury and medications<sup>3</sup>, but the molecular and cellular mechanisms behind these differences remain to be fully explored and psychiatric patients continue to be treated according to a "unisex-model"<sup>2</sup>.

From a cellular and molecular point of view, ELS has been shown to directly influence both the nervous and immune systems, triggering the systemic and local release of stress signals and inflammatory cues that can be detected by the main innate immune effectors of the brain parenchyma - microglia cells. Both the post-natal and the adolescent brain experience crucial remodelling events that rely on neurogenesis, migration and correct placement of specific neuronal populations, selective and activity-dependent neuronal elimination<sup>4</sup> and synaptic pruning<sup>5,6</sup> and myelination of axonal tracts<sup>7,8</sup>. Microglia cells are key players in all these processes, promoting neuronal clearance and synaptic refinement through phagocytosis<sup>9</sup> and secreting key factors for neurogenesis, neuronal migration and oligodendrocyte precursor cell (OPC) proliferation and maturation to full myelinating cells<sup>8</sup>.

Microglia, as an intrinsic part of the immune system, are also the main responsible for defending the brain parenchyma from external and internal threats. Thus, they have evolved to recognize changes in the delicate chemical environment of the brain and to mount an immune response adequate to the nature of the perceived danger. However, the different immune responses emerging in the presence of inflammatory triggers, such as those resulting from ELS exposure, come at a cost, causing profound phenotypic changes in microglia that can compromise the intrinsic homeostatic activity of these cells. In this context, we hypothesized that ELS may interfere with the ability of microglia to promote selective neuronal clearance and oligodendrocyte maturation during the first post-natal weeks, thus contributing to disrupt correct circuit wiring and potentiating maladaptive behavior responses, both in the early post-natal period and later in life.

In this project, we proposed to use a paradigm of early-life stress, known as the maternal separation and unpredictable stress model (MSUS), to study the impact of ELS on microglia-dependent circuit remodelling in the medial pre-frontal cortex (mPFC), with the ultimate goal of clarifying microglia:neuron and microglia:oligodendrocyte dynamics in the presence of optimal or sub-optimal maternal bonding experiences. We decided to focus our attention on the mPFC, since this brain region has been extensively implicated, both in rodents and humans, in stress response, impulse control and social behavior<sup>10,11</sup>. The mPFC is also known to be particularly susceptible to the effects of stress, as it is one of the last brain regions to fully mature, experiencing intense synaptic remodelling and myelination throughout the post-natal period until late adolescence. In addition, changes in neuronal activity, E/I balance and connectivity have also been reported in the mPFC of mouse models and patients diagnosed with different neurodevelopmental and neuropsychiatric diseases, including autism and schizophrenia, suggesting that this brain region may play a relevant role in the etiology of these diseases<sup>12</sup>.

## 2. METHODOLOGY AND AIMS:

### PART I: The MSUS paradigm and behavior analysis

#### 2.1 MSUS model

In order to understand the full impact of ELS exposure at the cellular, circuit and behavior level, we decided to employ the MSUS paradigm, which is designed to mimic both maternal neglect and maternal stress during the early life period. The MSUS protocol consists in the daily separation of the female from the litter from P2 to P14 (**Figure 1A**). The separation lasts for a 3h period, which occurs at a random time between 6 pm and 3 am (during the active period of the animals). During this period, the pups are kept together in a clean separate cage in the same room as the dam (**Figure 1B**), and the dam is subjected to one of two forms of stress (also randomly selected): forced swimming for 6 min in a water filled beaker or movement restraint for 20 min (**Figure 1C**). Importantly, in addition to the maternal separation imposed upon the dame and the pups, this paradigm adds the unpredictable stress component, which helps prevent compensatory maternal behaviors once the dam returns to the nest.

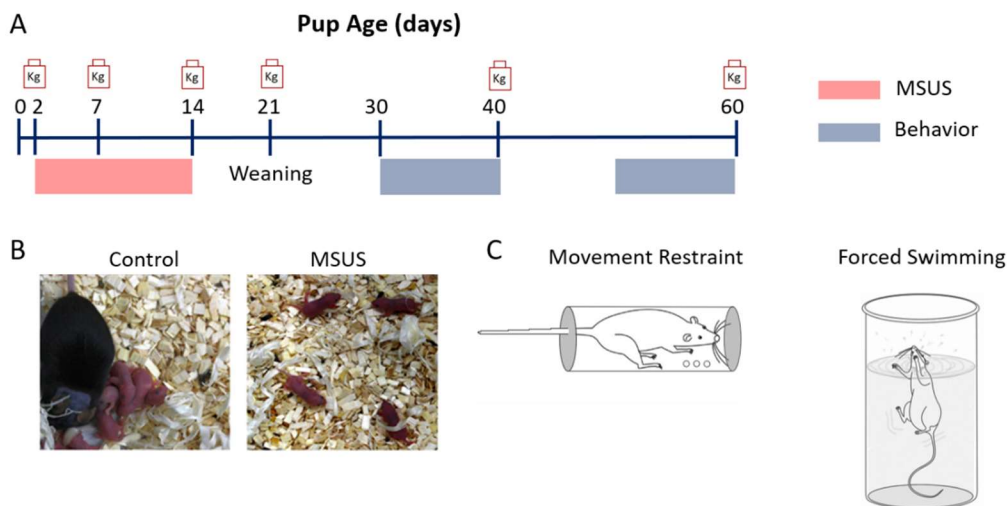


**Figure 1 – The MSUS protocol.** **A)** Timeline of the MSUS protocol. **B)** Control and MSUS litters during the separation period. **C)** Scheme of the movement restraint and forced swimming stress protocols to which dams are exposed during the 3h separation period.

#### 2.2 Pup retrieval test and maternal behavior

In order to validate this model and identify any behavior changes elicited by ELS in both the dam and the pups during the MSUS period (P2-P14), the pup retrieval test was performed at P2, P4 and P6, in both MSUS and control cohorts, and maternal behavior was recorded for 30 min after the test and also for 30 min after the separation period. The pup retrieval test consists in removing all pups from the home cage for 30 min and reintroducing them after this period one by one. The time the dam takes to recover the first 3 pups (placed in the

corners of cage, far away from the nest) and place them back in the nest is recorded, as well as the time the dam takes to pick and retrieve the first pup and the time she takes to collect all pups and to settle in the nest. During the 30 min recording sessions, before and after the separation period, the dam is observed and her behaviors are registered and classified according to the following table:

Behaviour	Description	Categorization
Licking/grooming	Dam touches the pup's body with her tongue/handles the pup with her forepaws or nose	Caring behaviour
Active nursing	Dam is in an arched back posture over the pups which are attached to the nipples	Caring behaviour
Passive nursing	Dam lies immobile on pups	Caring behaviour
Nest building	Dam collects and/or handles nesting material around the pups with mouth or forepaws	Caring behaviour
Self-grooming	Licking, brushing or scratching fur or paws with tongue	Self-maintenance
Eating/Drinking	Chewing food, sawdust or feces/licking water from bottle tip	Self-maintenance
Climbing/Digging	Dam climbs the cage lid/uses forepaws to scratch sawdust away from her body	Neglecting behaviour

### 2.3 Pup ultravocalization recordings

Pup ultravocalization recordings were also performed at P3, P5 and P7, before the beginning of the separation period. For this purpose, each pup was removed from the nest and placed in a sound-isolated box for a 6 min period, during which the vocalizations were recorded. For this analysis, the total number of vocalizations emitted by each pup, as well as the type and complexity of each one was evaluated using the software UltraVox (Noldus, Netherlands) and classified according to a previously defined scale that takes into account the shape and duration of each vocalization.

### 2.4 Social behavior evaluation

Since the mPFC is intimately related with social behavior and hierarchy, we investigated the social preference and social memory of MSUS and control mice, focusing on the adolescence period (P40), using the three-chamber test (3CT). A three-chamber arena was from Stoelting (Stoelting, Ireland) was employed in this study. The 3CT assay consisted of three sessions: the first session began with a 20-min habituation period during which the subject mouse freely explored all three chambers; next, the mouse was confined to the centre chamber and an empty wire cage (Empty) and a caged with an unfamiliar mouse (Stranger 1) were introduced to the side-chambers; in the second session, the subject mouse was then allowed to freely explore all three chambers for 10 min. Following the 10-min session, the animal remained in the chamber for an extra 10 min (post-test) to better acquire the identification cues from 'S1' animal. Before the third and last session, the subject mouse was gently guided to the centre chamber while the empty wire cage was replaced with a caged stimulus mouse (Stranger 2). In the last session, the subject mouse was then left explored all three chambers for 10 min. Stimulus mice were age-matched and sex-matched animals, previously habituated to the wire cages. The positions of the empty cage and stimulus-containing cages were alternated between tests. Time spent in close proximity, distance travelled, and heat maps were calculated using the automated software Ethovision XT (Noldus, Netherland).

### 2.5 Anxiety and depressive-like behavior evaluation

ELS exposure can lead to an increase in anxiety and depression in humans. To test if the MSUS model led to similar behaviors in rodents we employed two different tests in adolescent mice (P40): 1) the **forced swimming test**, which allows to evaluate animal resilience and despair behaviors, and 2) the **elevated plus maze**, designed to measure anxiety.

The forced swimming test (FST) was performed in a 2 L glass beaker (19 cm high with a diameter of 13 cm) filled with water (at  $18 \pm 1$  °C) up to 1,5 L. Testing started by introducing each mouse in a beaker and recording the animal's behavior for 6 min. Indirect and homogeneous illumination of the room was provided by white LED lamps at 20 lx. Latency to stop swimming and total time spent immobile were evaluated. Immobility was defined as the lack of motion of the entire body, except small movements to keep mouse head above water.

The elevated plus maze (EPM) consisted of a plus-shape apparatus with two open arms (without walls) and two closed arms (with walls), each one with 30 x 5 cm. Mice were placed at the center of the apparatus, facing one of the closed arms, and behavior was video-tracked automatically using Ethovision XT (Noldus, Netherlands) for 10 min. Direct illumination of the maze was provided by white LED lamps with open arms illuminated at approximately 300 lx. Time spent in the open arms and latency to enter an open arm were quantified automatically.

## **PART II: Characterization of microglia phenotype and function following MSUS exposure**

### **2.6 Tissue processing and immunohistochemistry**

Juvenile (P10) and adolescent (P40) MSUS and control mice were deeply anesthetized with isoflurane (Abott, USA) and perfused transcardially with approximately 20 mL of ice-cold phosphate buffered-saline (PBS). Whole brain was dissected and post-fixed overnight in 4% paraformaldehyde and afterwards transferred to a solution of 30% sucrose in PBS for cryopreservation and frozen at -80°C until further processing. Coronal sections of 50 µm were serially cut using a cryostat (Thermo scientific CryoStar NX50) and all slices encompassing the mPFC were collected into 48 multi well plates with Azide 0,02% in PBS and stored at 4°C until further processing.

Microglia cell morphology and lysosome content was assessed by **fluorescence immunohistochemistry**, employing primary antibodies against microglia-specific marker IBA-1 and lysosome marker CD68. The immunohistochemistry protocol was performed in free-floating sections (10 sections/mouse, equally spaced by 150 µm) processed in 12-well multi-well plates (6 sections/well). Sections were first washed for 5 min in PBS to remove azide and then blocked and permeabilized (1h at room temperature) in a solution of 10% goat serum, 0.1% Triton in PBS. The slices were then incubated overnight at 4°C with rabbit anti-Iba1 antibody (1:1000) (Wako, USA) and goat anti-CD68 (1:500) (Bio-Rad, USA) in the same blocking solution, under constant agitation. On the next day, sections were washed 3 times with PBS (5 min, 3x) and incubated with the necessary secondary antibodies: Alexa Fluor 488 goat anti-rabbit and Alexa Fluor 647 goat anti-rat (1:200) (Life-Technologies, USA), for 2h at room-temperature, also under constant agitation. The sections were then washed again 3 times in PBS and mounted onto gelatinized microscope slides using Vectashield hardSet Mounting Medium with DAPI (Vector Laboratories, USA).

For stereology, **transmission immunohistochemistry** was performed using the same anti-IBA-1 antibody (1:1000). The immunohistochemistry protocol was performed in free-floating sections incubated in 24 multi-well plates (10 sections/mouse, equally spaced by 150 µm). Briefly, sections were incubated for 30 minutes at 37°C with phenylhydrazine to quench peroxidase activity. Following 3 washing steps with PBS, sections were blocked and permeabilized with 10% normal goat serum (Thermo Scientific, USA), 0,1%Triton in PBS for 1h at room temperature and then incubated with the primary rabbit anti-IBA-1 antibody (Wako, USA) 1:1000 in the same blocking solution, at 4°C over-night, under constant agitation. On the next day, sections were washed 3 times with PBS and incubated with the secondary biotinylated antibody anti-rabbit IG (Vector Labs, USA) 1:200 for 2h at RT, also under constant agitation. Following another washing step with PBS, bound antibodies were visualized using the VECTASTAIN® ABC kit (Vector), according to the instructions of the manufacturer, and 3,3'-diaminobenzidine tetrahydrochloride (DAB metal concentrate - Vector) was used as substrate. After washing with PBS, brain sections were mounted on microscope slides, subjected to dehydration with an ethanol gradient and xylene and covered with Eukitt® (PanReac AppiChem, USA) mounting medium and a microscope coverslip.

### **2.7 3D reconstruction and morphological analysis of microglia cells**

For morphological analysis, mounted brain sections of P10 and P40 animals were visualized in a 710 LSM confocal microscope (Zeiss) with a Pln Apo 40x/1,4 DIC lens, employing the Zen Black software (v2.6, Carl Zeiss, USA). At least 4 mice per condition were analysed and, in each mice, Z-stacks from at least 10 mPFC microglia cells were acquired. Each image was a compilation of images taken across the Z plane of the sections with a step of 0.6  $\mu\text{m}$  (between 20 to 40 planes per cell). Confocal microscope settings were kept the same for all scans. Microglia cells were traced and reconstructed using the surface and filament tools from the Imaris software (v7.4.2, Oxford Instruments, UK). Surface analysis was used to calculate the total area, volume, and ellipticity of each cell, as well as CD68 total area, volume and n<sup>o</sup> of CD68 particles. Filament analysis allowed to perform a 3D reconstruction of microglia branches in order to perform sholl analysis and determine branch parameters.

## **2.8 Stereology**

An unbiased stereology-based approach was used to count microglia cells (P10 and P40 animals) and PV-TdTomato<sup>+</sup> neurons (P40 animals) in all sub-regions and layers of the mPFC. For each animal, 10 random sections, with a fixed distance of 150  $\mu\text{m}$  between each other, were analysed. A number code was attributed to each animal to ensure blinding of the investigator performing the stereology analysis. Unbiased stereology estimation of microglia cells was performed using the commercial software Stereo Investigator (v 2018.1.1, MBF Bioscience, USA). Following IBA-1 staining, sections were visualized under an Axio Imager 2 microscope (Carl Zeiss, Germany) and the regions of interest (ROIs) were identified in each section. For microglia stereology, ROIs corresponding to Medial Orbital Cortex (MO), Pre-Limbic Cortex (PrL), anterior Cingulate Cortex1 (CG1) and Infralimbic Cortex (IL) regions were selected in each slice, while for PV-TdTomato neuron stereology, each of the mPFC regions was further sub-divided accordingly to cortical layers, in order to obtain 3 ROIs corresponding to layer II/III, layer V and Layer VI. Microglia cells were counted using a sampling grid of 160 x 160  $\mu\text{m}$  and a counting frame of 80 x 80, while TdTomato neurons were counted a sampling grid of 75 x 75  $\mu\text{m}$  and a counting frame of 50 x 50. The same sampling and stereology parameters were used for all ROIs and in all animals and an area sampling fraction of 0,19 and an error coefficient bellow 0,05 was achieved.

## **2.9 mRNA quantification by qRT-PCR**

RNA brain samples from P10 and P40 control and MSUS mice were extracted to identify possible genetic correlates of ELS effects on microglia and behavior. Following animal sacrifice, brains were dissected and the mPFC was collected and immediately frozen and stored at -80°C until further processing. Total RNA was purified from the mPFC using the NucleoSpin<sup>®</sup> Total RNA extraction kit (Macherey Nagel, USA), according to the manufacturer's protocol. During the procedure, a step of elimination of genomic DNA was performed in the silica columns using the DNase provided with the kit. Samples were eluted in 30  $\mu\text{L}$  of RNase free water and concentrations were measured in a Nanodrop 2000 spectrometer (Thermo Scientific). Samples were stored at -80°C until gene expression analysis. For quantification of gene expression, 250 ng of total RNA were transcribed using the NZYtech First-Strand cDNA Synthesis Kit (NZYTech, Portugal). cDNA was diluted 20x before preparation of the qRT-PCR reactions. The relative expression of each gene of interest was quantified by qRT-PCR using the NZYSpeedy qPCR Green Master Mix (NZYTech) and pre-designed primers. Briefly, the mixture of cDNA sample and master mix (per primer) was heated at 95°C for 2 minutes, followed by 40 cycles of 5 seconds for the annealing of primers at 58° or 60° (depending on the melting temperature of each primer set) and 30 seconds for amplification at 72°C. After amplification, a melting curve protocol was performed with 1-minute heating at 55°C followed by 80 steps of 10 seconds with a 0.5°C increment until reaching 90°C. All reactions were performed in duplicate in a StepOne<sup>™</sup> Plus device (Thermo Fisher). A standard curve was prepared for each gene, using 10x, 50x and 100x dilutions from a control sample, in order to determine the efficiency of each primer set. Two negative controls (no reverse transcription – NRT and no target control – NTC) were run for each gene. The gene HPRT was used as reference gene throughout this study. Calculation of mRNA fold change for each gene were performed according to the Pfaffl Method.

### 3. MAJOR RESULTS AND DISCUSSION:

In order to gain a clear picture of the potential impact of ELS exposure on mPFC wiring and microglia activity, we decided to study two different and critical time-points of mPFC development, the first corresponding to the period between **P5-P10 (juvenile period)**, during which clearance of inhibitory neurons is occurring in the different layers of the mPFC, and the second corresponding to **P35-P40 (late adolescence)**, a time point during the final maturation of mPFC circuits, when synaptic remodelling and the last stages of myelination are well underway. The first period of evaluation (P5-P10) allowed us to investigate the acute effects of ELS both on pup and maternal behavior and, at the cellular level, on microglia transcriptome and morphology, since it fell within the time-frame of the MSUS protocol. On the other hand, the second period of evaluation (P35-P40) was distant from the protocol and occurred at a point in time where the animals were already weaned (P21) and separated from their mothers. This time point was critical to help us fully characterize the long-term behavior changes triggered by ELS exposure, as well as to identify changes in microglia phenotype that could help explain these changes, in both adolescent and adult animals.

In our analysis, we also paid close attention to possible sex-driven differences at the molecular, cellular and behavior level, since several studies have reported different behavior outcomes and cellular differences in male and female rodents exposed to stress paradigms and several neurodevelopmental and neuropsychiatric disorders associated with mPFC dysfunction present a strong sex bias.

#### Part I – Behavioural characterization of the MSUS model.

We started our study by analysing the acute impact of ELS on maternal-pup interaction. In order to accomplish this, we performed regular weight assessments, in control and MSUS litters, during the MSUS period and until P40, in order to understand the possible consequences of ELS to pup feeding and weight-gain. We also performed the pup retrieval test at P4 and P6 and evaluated maternal-initiated behavior immediately after the pup retrieval protocol at these two time points.

All pups used in this study were weighted at P2, P7, P14, P21 and P40. It was possible to observe that both male and female MSUS pups showed a decrease in total body weight until P40 (**Figure 2A and 2B**). However, this decrease was smaller in males than in females and no longer present in adulthood (see Franco et al, under revision). This temporary loss of weight is probably related with a decrease in nursing time, since MSUS dams were absent for 3h/day and, even when they were in the cage, tended to spend less time in the nest, with respect to control dams. Despite being exposed to stress paradigms between P2 and P14, we did not observe significant differences in the time the MSUS dams took to pick the first pup (**Figure 2C**) or retrieve all pups (**Figure 2D**) and place them back in the nest during the pup retrieval test. However, we observed a decrease in the time MSUS dams spent handling the pups during this test (**Figure 2E**). In addition, when we analysed the behavior of the same dams immediately after the end of the pup retrieval protocol (**Figure 2F**), we observed that at P4 MSUS dams spent more time outside the nest performing neglecting behaviors, such as digging and climbing, than control dams. This behavior was less evident at P6, suggesting an improvement of maternal care over time, even for MSUS dams. Nevertheless, overall, these results suggest that dams exposed to maternal stress during the early post-natal period are less prone to sustain caring maternal behaviors necessary for pup feeding and well-being.

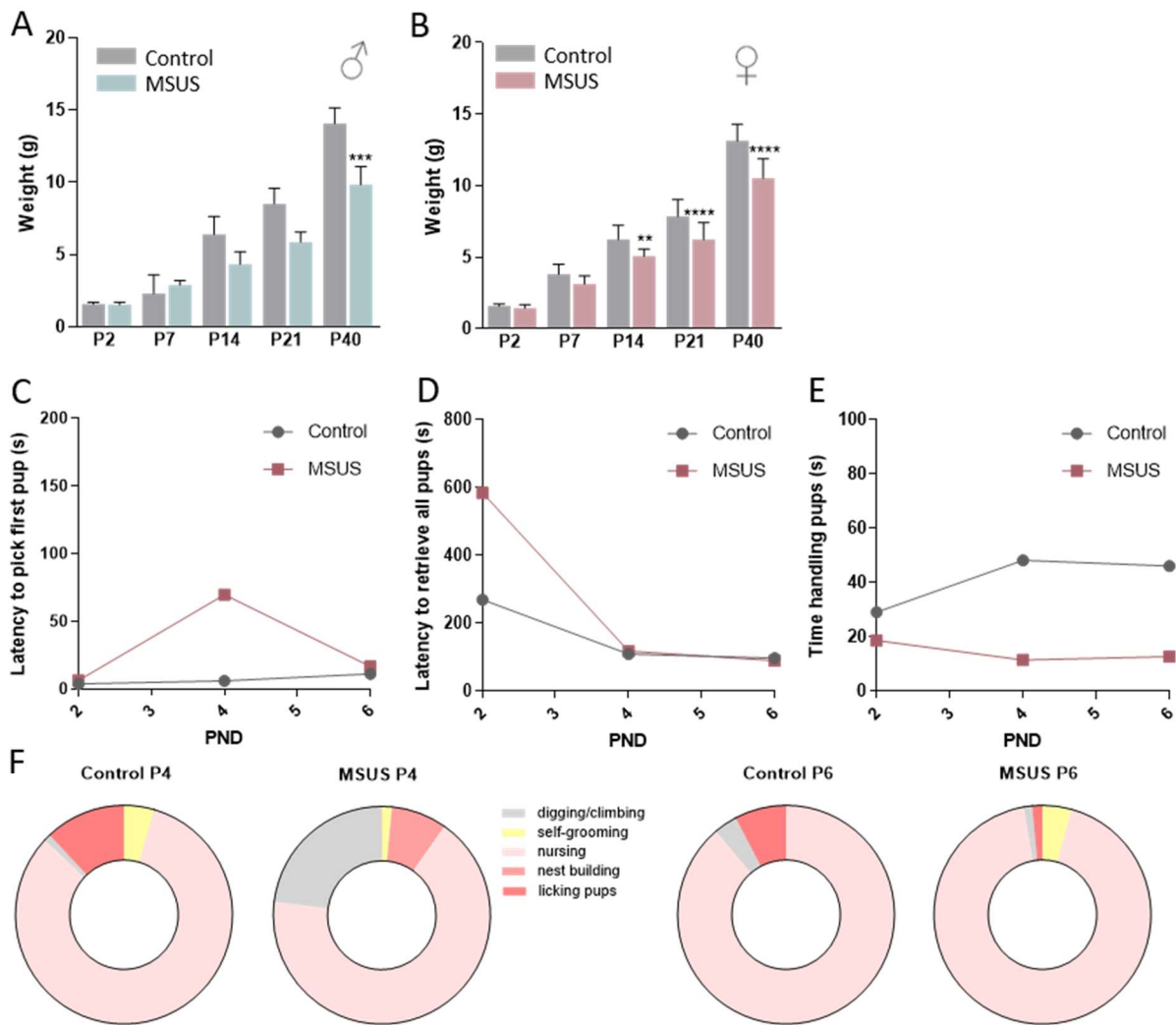


**Figure 2 – MSUS leads to decrease mouse weight and poorer maternal care.** **A** and **B**) All pups were weighted at P2, P4, P14, after weaning and before animal sacrifice (P40). **A**) MSUS male and **B**) female pups displayed a significant decrease in body weight, with respect to controls. Results are presented in grams (g) and are representative of at least n=7 for males and n=13 for females. **C**) Latency to pick the first pup, **D**) latency to retrieve all pups and **E**) time spent handling pups were evaluated during the pup retrieval test. Results are presented in seconds (s) and are representative of at least two litters per condition. **F**) Maternal behaviors were evaluated during a 30 min video recording performed immediately after the pup retrieval test. The graphs represent the % of total time dams presented caring behaviors (nursing, nest building and licking pups), self-maintenance (self-grooming) or neglecting behaviors (digging or climbing). \*\*  $P \leq 0.01$ , \*\*\*  $P \leq 0.001$ , \*\*\*\*  $P \leq 0.0001$  with respect to Control groups, according to Two-way ANOVA. Data are presented as means  $\pm$  SEM.

In order to understand if the decrease in maternal care presented by MSUS dams directly interfered with pup neurodevelopment and behavior and since it has been previously described that early developmental disruption of corticostriatal circuits can compromise social communication by affecting motor routines such as those required for the generation of ultrasonic vocalization, we measured the number ultravocalizations emitted by control and MSUS pups at P3, P5 and P7, during a period of 6 min in which the pup was separated from both the dam and the litter (**Figure 3A and 3B**). We also classified each vocalization recorded at P5 and P7 according to its shape and complexity (**Figure 3C and 3D**).

As expected, our analysis revealed that the total number and the overall complexity of vocalizations emitted by the both control and MSUS pups increased with age. In addition, the number of vocalizations was higher in females than in males, particularly at P3, suggesting that females develop the capacity to perform this form of communication earlier in development than males. Interestingly, we detected a reduction in the number of complex calls in female MSUS mice, both at P5 and at P7, with respect to control females. Although these results are not yet statistically significant due to the small number of tested animals, they are quite striking. In male MSUS animals, not only the number of complex calls was much smaller than in females at both ages, but there was almost no increase in this type of vocalizations between the two time points. These results suggest that

exposure to ELS may interfere with the maturation of the corticostriatal circuits responsible for ultrasonic vocalization, leading to a delay in the development of this form of communication.

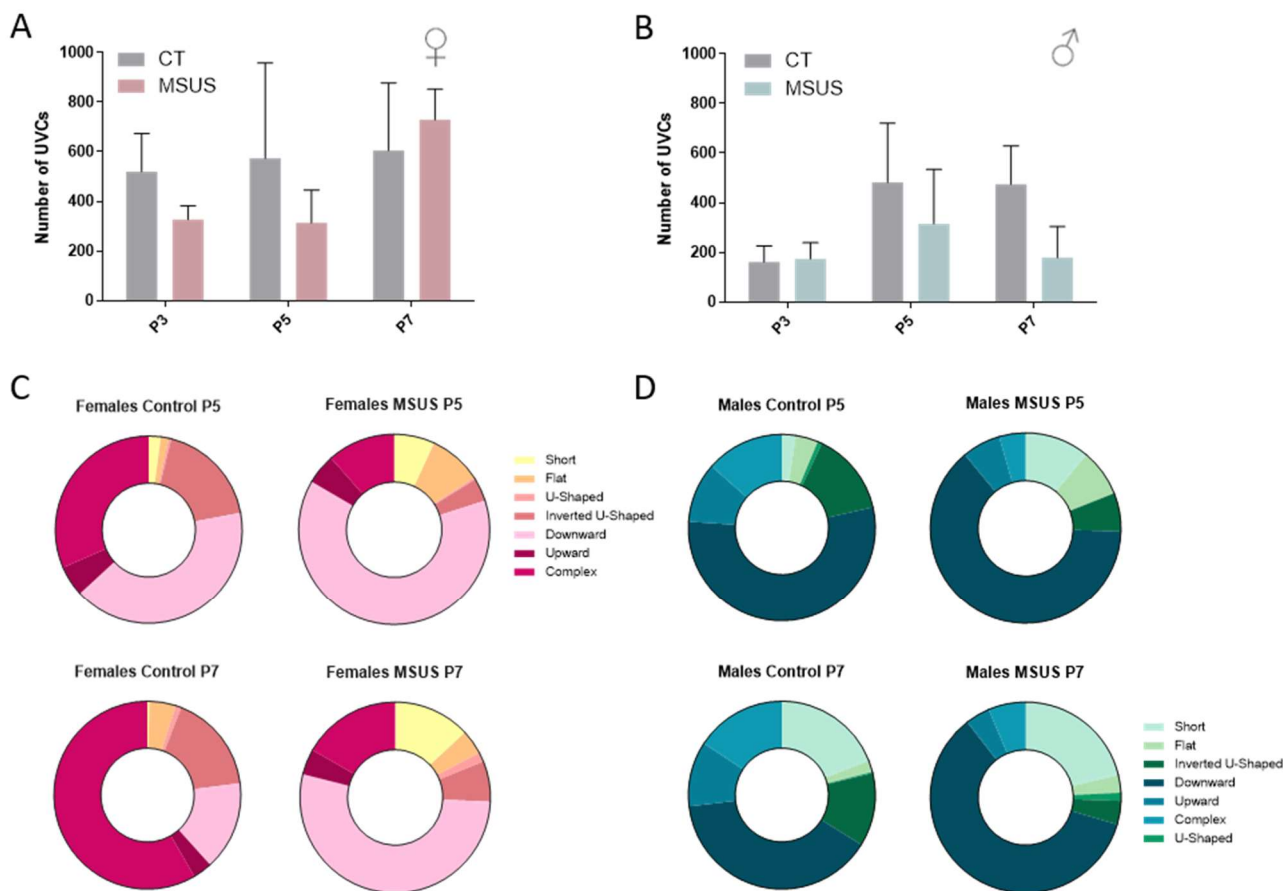


**Figure 3 – MSUS leads to a decrease in the number and complexity of ultrasonic vocalizations.** A and B) The total number of emitted calls in a 6 min period was determined for each mouse at P3, P5 and P6. A) MSUS female and B) male pups displayed a tendency for a reduction in the total number of calls, with respect to controls. C) and D) The type and complexity of each vocalization was analysed using the UltraVox software. It was possible to observe a tendency for a reduction in the number of complex vocalizations in male and female MSUS mice with respect to controls, both at P5 and P7. Results are presented in n° of vocalizations/6min and are representative of n=2 for control females, n=5 for MSUS females and n=3 for male control and MSUS mice.

In order to investigate if ELS exposure could lead to long-term changes in social behavior, we performed several behavioral assessments both in adolescent and adult MSUS mice, using different paradigms designed to evaluate social interaction, social rank, anxiety and depressive-like behavior. Our more striking observation was that adult male MSUS mice tended to display a long-lasting submissive phenotype, increased social recognition and enhanced explorative behavior (see Franco et al, under revision). We were able to correlate this decrease in social rank with dendritic atrophy and greater amplitude of inhibitory synaptic inputs in pyramidal neurons from the medial prefrontal cortex. Using gene expression analysis and electrophysiological recordings we pinpointed NPY1R signalling as the driver of these enhanced GABAergic currents. Overall, our findings uncovered that exposure to early life stress leads to striking remodelling of prefrontal network function, along with neuronal and gene expression changes that lead to social behavioral adaptations in adult life. Based on these findings, we decided to investigate if changes in social behavior could already be observed during adolescence, a critical time point for mPFC maturation and remodelling. For this purpose, male and female MSUS and control animals were subjected to several behavioural tests to assess social interactions, depressive-like behaviour and anxiety/risk-taking behaviours between P35 and P40.

In what concerns social behaviour, we performed two different evaluations employing the 3 chamber paradigm (Figure 4): 1) the social preference test, which explores the social nature of mice by exposing the animal to an empty cage or a cage with a stranger mouse, and 2) the social novelty test, which allows evaluation of social memory, by exposing the test mouse to the previous social stimulus (social 1) and to a new social stimulus (social

2). In the first part of the test, as expected, we observed that both female (**Figure 4A**) and male control (CTR) mice (**Figure 4C**) preferred to interact with the social stimulus (social 1), spending significantly more time in the chamber that had the cage with the animal inside. A similar behavior was observed for female MSUS mice, which did not present differences in the social preference index (**Figure 4E**). However, this social preference was not as clear for male MSUS mice, which, despite spending more time with the social partner, presented a lower social preference index, when compared to controls (**Figure 4H**). In order to investigate if the decrease in social preference observed in male MSUS animals was due to hyperactivity, we also measured the total distance travelled by the animals (**Figure 4F** and **4I**) and the instant speed (**Figure 4G** and **4J**). No significant differences were observed between MSUS and controls, although male MSUS animals show a tendency to travel less in the arena, spending more time still in each compartment, which might suggest an increase in anxiety. In the second part of the test, both female (**Figure 4B**) and male (**Figure 4D**) CTR and MSUS animals presented the expected behaviour, spending more time interacting with the novel mouse (social 2) than with the known animal (social 1), indicating that exposure to early life stress does not significantly impact social memory in the adolescence period.

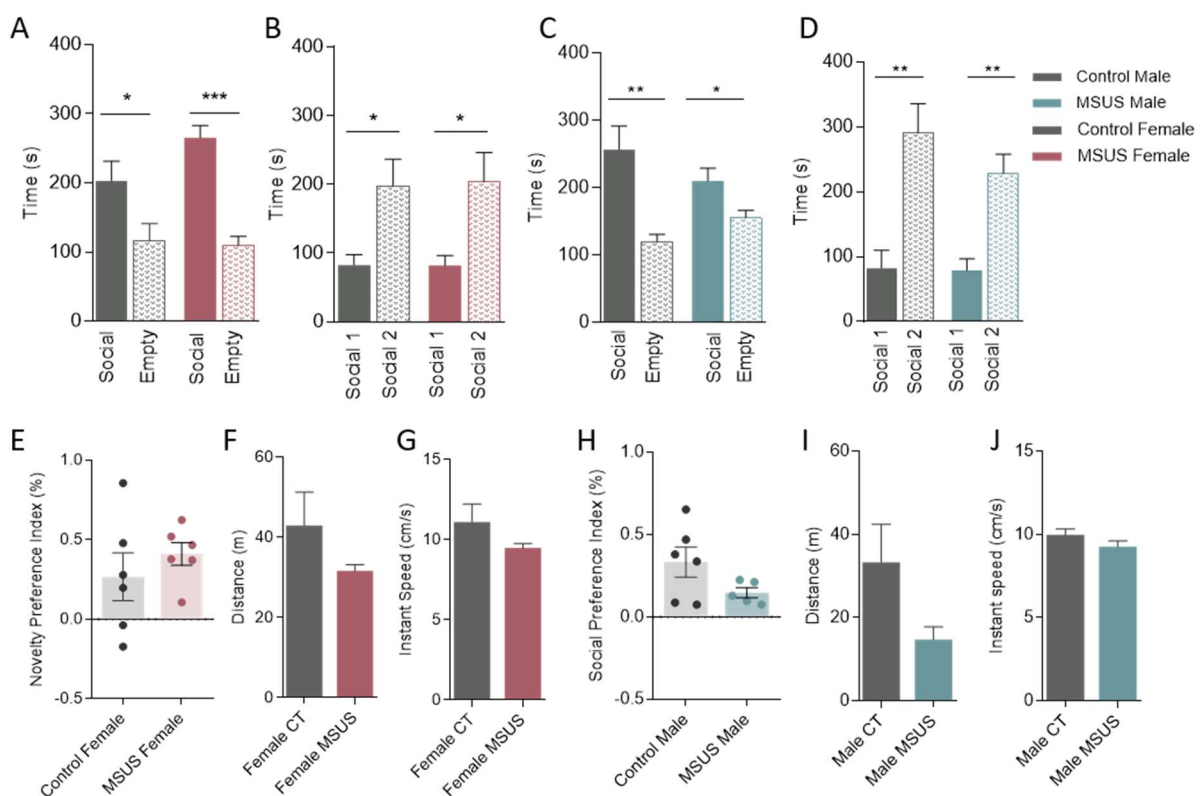


**Figure 4**

– **Social preference and social social memory in adolescent MSUS mice.** We employed the 3 chambers test to evaluate both social preference (A and C) and social memory (B and D) in PV-tdTomato MSUS and control mice between P35-P40. Time spent by female **A** and **B**) and male **C**) and **D**) CTR and MSUS mice in each compartment of the arena was measured and is represented in seconds (s). **E**) and **H**) Male but not female MSUS mice present decreased social preference, as observed by a reduced social preference index, but no changes in social memory. Furthermore, no changes in distance travelled (m) **F**) and **I**) or instant speed (cm/s) **G**) and **J**) were observed in female or male MSUS mice with respect to controls, suggesting that changes in social preference are not due to hyperactivity. At least n=6 for male and female mice in each group. \*P ≤ 0.05, \*\* P ≤ 0.01 and \*\*\* P ≤ 0.001 according to Mann-Whitney test. Data are presented as mean ± SEM.

We next decided to evaluate if exposure to the MSUS paradigm led to changes in anxiety levels and depressive behaviors in adolescent mice, as previously observed in adult males. For this purpose, we performed two different tests: 1) the elevated plus maze (**Figure 5A-D**), which addresses anxiety and also risk-taking behaviours, and 2) the forced swimming test (**Figures 5E-F**), which evaluates depressive and despair behaviours.

Similarly to what was observed in adult male mice (see Franco et al, under revision), both male and female MSUS animals presented a lower latency to enter the open arms of the EPM (**Figure 5A** and **5C**), suggesting that exposure to ELS can increase risk taking behaviors later in life. This result is particularly striking and statistically

significant in female MSUS, who not only quickly enter the open part of the maze but also spent more time in the open arms with respect to sex-matched controls (**Figure 5B**). In addition, while we previously observed that adult male MSUS animals present an increase in despair behaviors in the forced swimming paradigm, suggestive of a depressive-like phenotype, we could not recapitulate this observation in adolescent male mice and even observed a the reverse behavior in P40 female MSUS animals, which presented significantly higher latencies to stop swimming (**Figure 5E**) with respect to controls. Overall, our results suggest that ELS exposure leads to an increase in risk taking behavior and does not trigger significant anxiety or depressive like behavior during the adolescence period. Moreover, ELS generates resilience in female adolescent mice, which may help explain why females seem less susceptible to ELS behavior outcomes in adulthood.

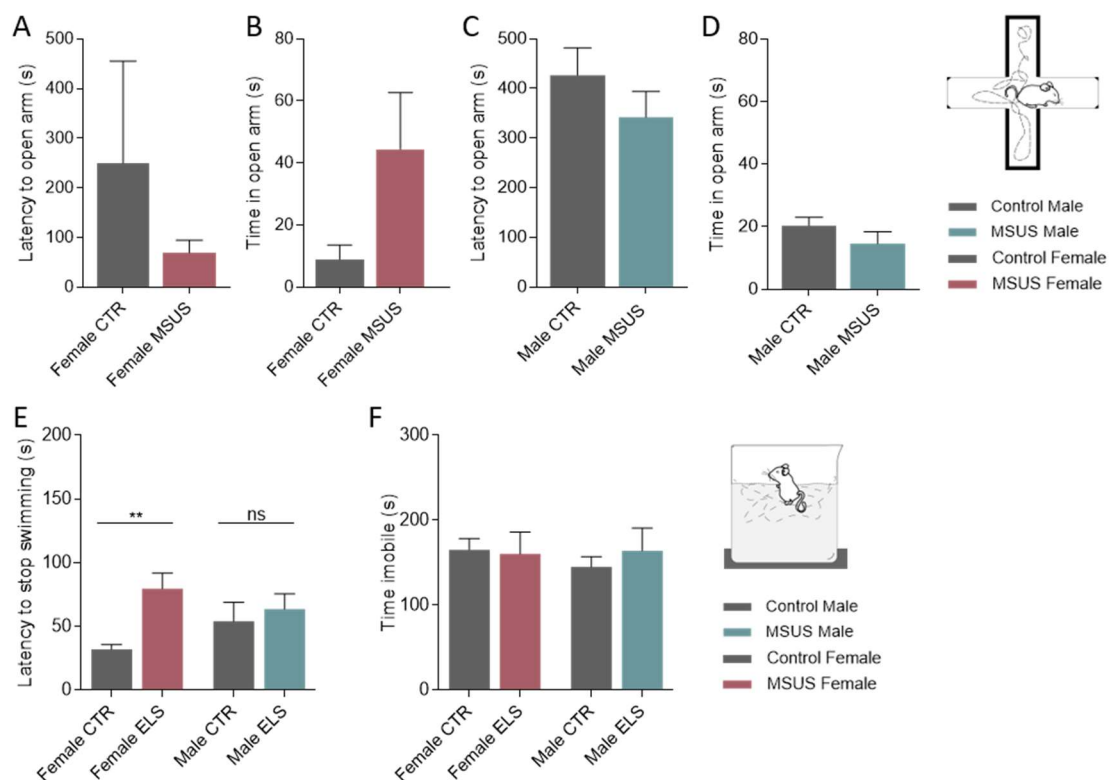


**Figure 5 – Anxiety and despair behaviours in juvenile MSUS mice.** The effect of ELS exposure on anxiety, risk-taking and despair behaviours was assessed in male and female PV-tdTomato control and MSUS animals between P35-P40, by the elevated plus maze (EPM) and forced swimming test, respectively. **A** and **C**) Latency to enter the open arm and **B** and **D**) time spent in the open arms are expressed in seconds (s). **A**) Female and **B**) male MSUS mice present a decrease in the latency to enter the open arm. Anxiety and despair behaviours were also evaluated using the forced swimming test. **E**) The latency to stop swimming and the **F**) time spent immobile are expressed in seconds (s). Female MSUS mice, but not male MSUS mice, present an increase in the latency to stop swimming with respect to controls, suggesting a decrease in despair-like behaviours. At least n=6 for male and female mice in each group. \*\* P ≤ 0.01 according to unpaired t-test with Welch’s correction. Data are presented as mean ± SEM.

## Part II – Characterization of microglia morphology and function

In order to understand the acute and long-term impact of ELS exposure on microglia activity we performed an extensive characterization of microglia density, morphology and gene expression profile in the mPFC of male and female P10 and P40 mice, employing different microscopy and image analysis techniques.

Microglia cell density in the different subregions of the mPFC: the anterior cingulate cortex (ACC), prelimbic area (PL), infralimbic area (IL) and medial orbital cortex (MO) was determined by stereology, which is based on an unbiased mathematical extrapolation method. Although we did not find significant changes in cell density between control and MSUS mice across the mPFC, we observed that male animals presented a tendency towards a higher number of microglia cells than female animals in all subregions of the mPFC. This result is in line with previous observations in other brain regions, and correlates with the smaller size of male microglia

with respect to female microglia, suggesting that a higher number of microglia cells needs to exist in males in order to effectively to survey the same territory.

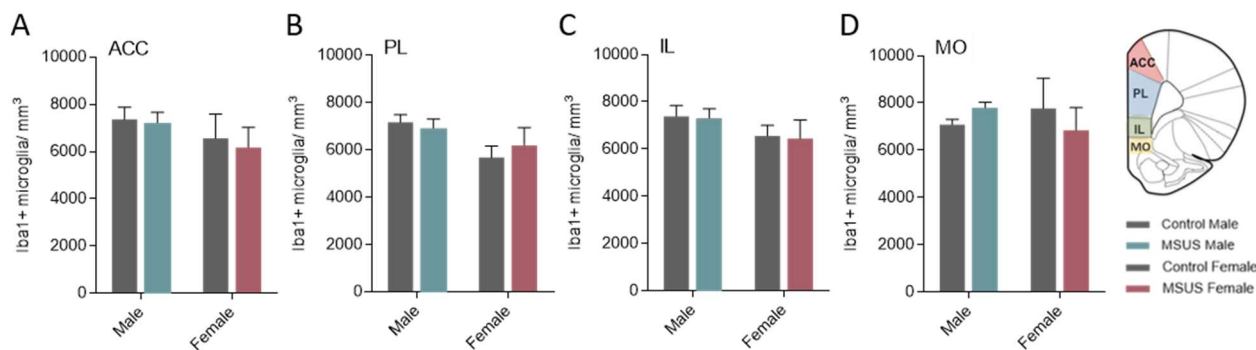


**Figure 6 – Stereology-based evaluation of total number of microglia cells in the mPFC.** The mPFC was divided in four sub regions; anterior cingulate cortex (ACC), prelimbic region (PL), infralimbic region (IL) and medial orbital cortex (MO). The total number of microglia cells in the total volume of each region was estimated by stereology, for each of the designated regions **A)** ACC **B)** PrL, **C)** IL and **D)** MO, using a Zeiss Z2 microscope and the StereoInvestigator software. No differences were observed in microglia cell density between control and MSUS animals. Results are expressed as the number of cell/mm<sup>3</sup> and are representative of at least n=7 for each experimental group. Data are presented as mean ± SEM.

In what concerns microglia morphology, we performed Sholl (**Figure 7**), filament (**Figure 8**) and surface analysis (**Figure 9**), following immunohistochemistry against microglia marker IBA-1 and lysosome marker CD68. We employed Imaris software to perform 3D reconstruction of individual microglia cells from z-stack images acquired through confocal microscopy. Sholl analysis revealed interesting age- and sex-dependent differences in control microglia, some of which were exacerbated by exposure to ELS. It was possible to observe that at P10 both male and female microglia were similar in terms of ramification number and overall size (**Figure 7A**). In addition, at this age, no significant differences were observed between MSUS and control animals (**Figure 7C** and **7D**), although a tendency for a decrease in ramification number close to the cell body was observed in male MSUS microglia (**Figure 7D**), while female MSUS microglia presented the opposite effect (**Figure 7C**). Interestingly, P10 microglia were considerably less ramified than P40 microglia (**Figure 7B**), indicating that these cells go through important morphological changes during the post-natal period, in order to reach the mature phenotype observed in adolescent and adult mice. These changes are suggestive of a “deactivation” process, compatible with the different microglia functions that have been described at the different ages.

Contrarily to what was observed in juvenile mice, sexual dysmorphisms were present following the onset of puberty, since P40 female control microglia were significantly more ramified than male microglia (**Figure 7B**). At this age, we could also identify important morphological changes triggered by ELS exposure. In females, the MSUS protocol resulted in a slight reduction of ramification number closer to the cell body (**Figure 7E**), while in males the opposite effect was observed (**Figure 7F**), with male MSUS microglia displaying a very ramified phenotype that resembled that of P40 female control microglia and a reduction in overall cell size. These results suggest that while ELS triggers acute changes in the microglia of female mice, the response in males appears to be delayed and is significantly more drastic.

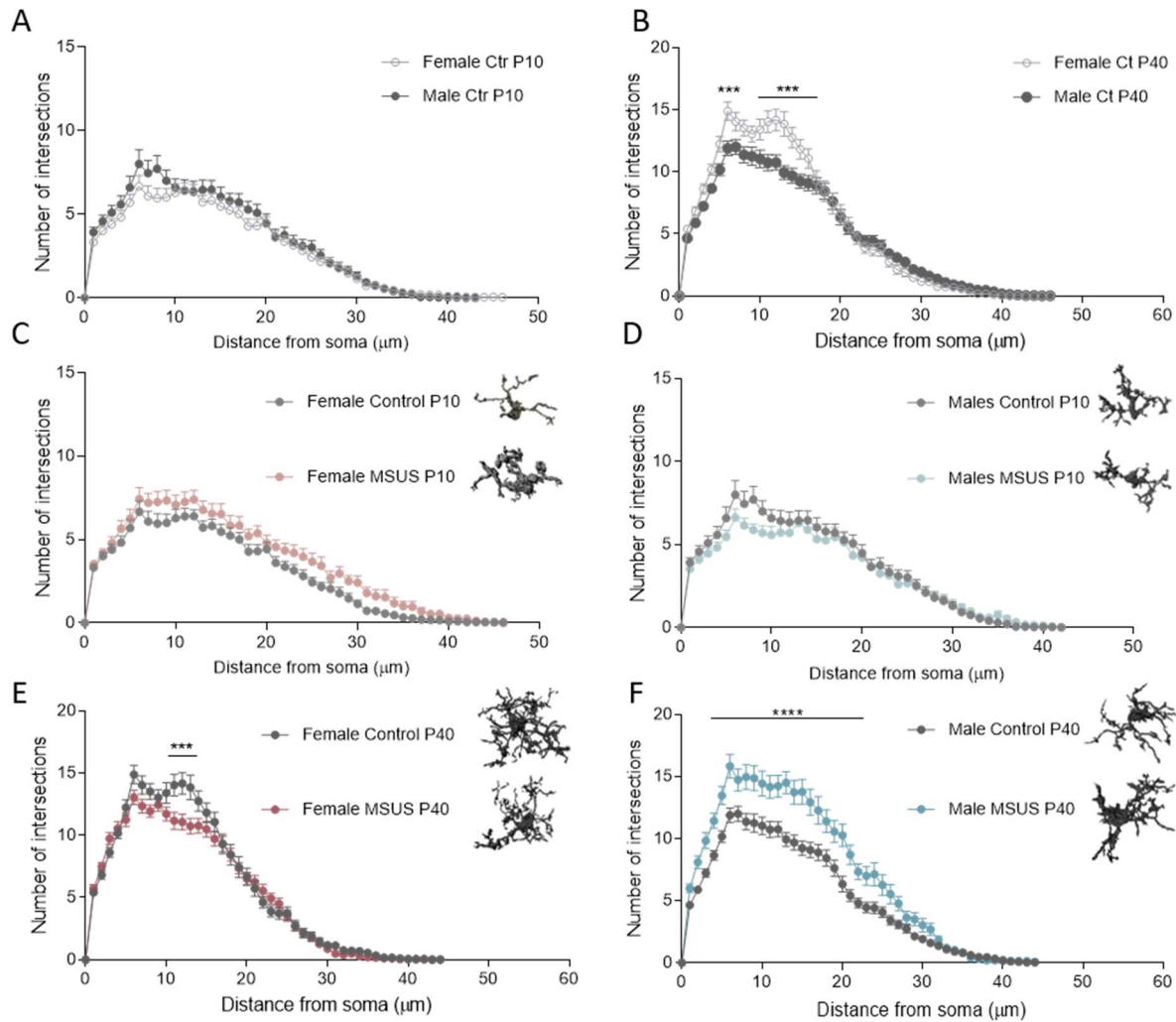


**Figure 7 – Sholl analysis of microglia cells in the mPFC.** Microglia from P10 and P40 male and female control and MSUS animals were observed under a confocal microscope following Iba-1 immunohistochemistry. Z-stacks were collected of isolated cells in order to perform 3D reconstruction and Sholl analysis using the Imaris software. **A)** and **B)** present a comparison between male and female control cells at P10 and P40, respectively. A comparison between **C)** and **E)** female and **D)** and **F)** male control and MSUS animals was also performed at P10 and P40. Results are expressed as the number of ramifications found at a variable distance from the cell soma and are representative of at least n=40 cells and n=4 animals per experimental group. \*P ≤ 0.05, \*\*P ≤ 0.01, \*\*\*P ≤ 0.001 \*\*\*\*P ≤ 0.0001 according to two-way ANOVA followed by Tukey's post hoc test. Data are presented as mean ± SEM.

We next employed filament (**Figure 8**) and surface analysis (**Figure 9**) to perform a more in depth analysis of cell morphology. At P10, during the MSUS paradigm, male mice showed only discreet changes in microglia morphology, such as a slight increase in the number of branching points (**Figure 8E**), as well as tendency for a decrease in total cell area and volume (**Figure 9A** and **9C**) and an increase in Iba-1 intensity (**Figure 9D**), suggestive of an activated phenotype. At this same age, changes in female MSUS animals were more profound. Female MSUS microglia presented an increase in filament length and volume, as well as a higher number of branching and ending points (**Figure 8**). These results are in agreement with the tendency previously observed in the Sholl analysis and indicate an acute response to ELS exposure that is characterized by an hyper-ramified morphology.

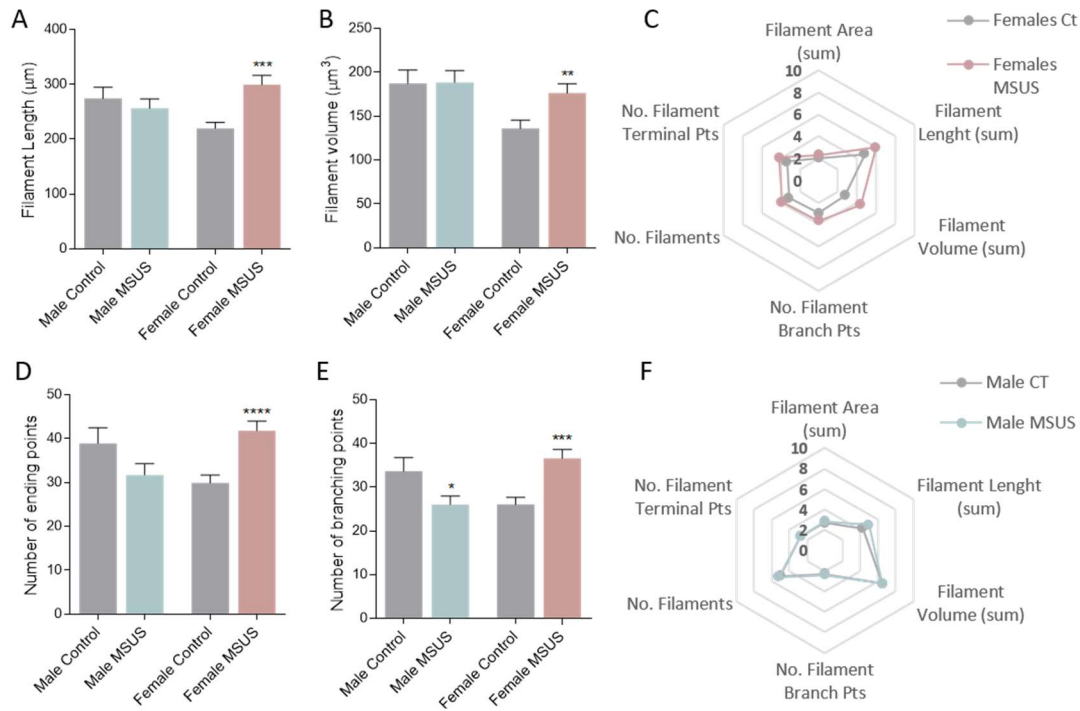


**Figure 8 – Filament analysis of microglia cells in the mPFC of P10 control and MSUS mice.** Microglia from P10 male and female control and MSUS animals were observed under a confocal microscope following Iba-1 immunohistochemistry. Z-stacks were collected of isolated cells in order to perform 3D reconstruction and filament analysis using the Imaris software. Several parameters were compared between the experimental groups, including **A)** filament length (expressed in  $\mu\text{m}$ ), **B)** filament volume (expressed in  $\mu\text{m}^3$ ), **D)** number of ending points and **E)** number of branching points. **C)** and **F)** present radar plots for all parameters in A, B, D and E and also for filament area and nº of segments. Results are representative of at least n=30 cells for each experimental group. \* $P \leq 0.05$ , \*\* $P \leq 0.01$ , \*\*\* $P \leq 0.001$  with respect to sex-matched control group, according to unpaired t-test with Welch's correction. Data are presented as mean  $\pm$  SEM.

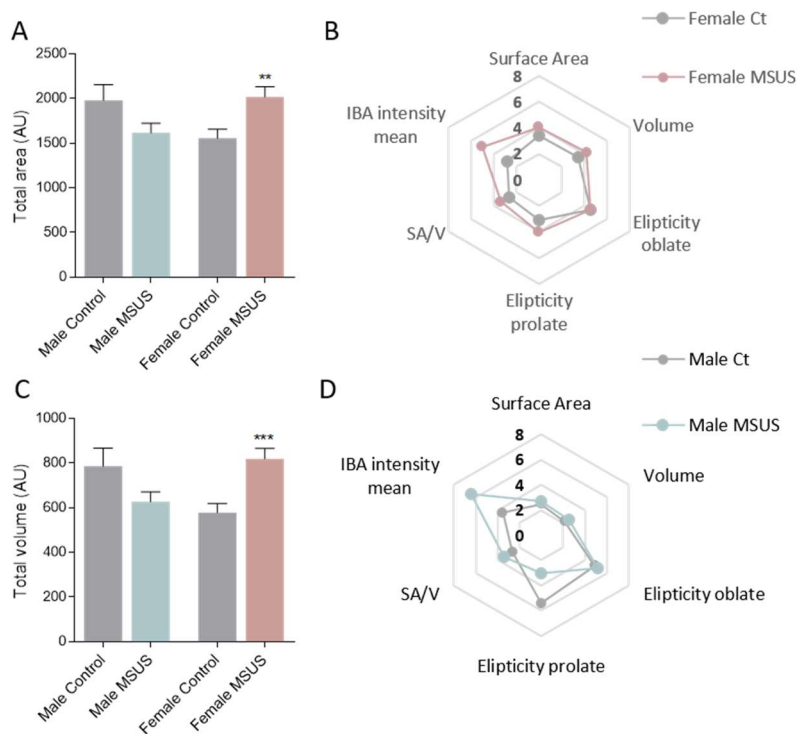


**Figure 9 – Surface analysis of microglia cells in the mPFC of P10 control and MSUS mice.** Microglia from P10 male and female control and MSUS animals were observed under a confocal microscope following Iba-1 immunohistochemistry. Z-stacks were collected of isolated cells in order to perform 3D reconstruction and surface analysis using the Imaris software. Several parameters were compared between the experimental groups, including **A)** total cell area (expressed in  $\mu\text{m}^2$ ) and **C)** total cell volume (expressed in  $\mu\text{m}^3$ ). **B)** and **D)** present radar plots for filament area and volume and surface area/volume ration, ellipticity, and Iba-1 intensity. Results are

representative of at least n=30 cells for each experimental group. \*\*P ≤ 0.01, \*\*\*P ≤ 0.001 with respect to sex-matched control group, according to unpaired t-test with Welch's correction. Data are presented as mean ± SEM.

At P40 (**Figure 10** and **Figure 11**), both filament and surface analysis clearly corroborated the results from Sholl analysis showing that, at this age, male mice are the ones displaying more profound changes in cell morphology as a result of previous exposure to the MSUS paradigm. Male MSUS microglia show a very significant increase in filament area and volume (**Figure 10D** and **10F**), as well as an increase in filament length (sum) (**Figure 10E**), as a result of their hyper-ramified morphology. They also show the expected increase in the number of branching and ending points (**Figure 10J** and **10K**). In addition, surface analysis revealed that these cells have an increase in total area (**Figure 11D**) and total volume (**Figure 11E**), with respect to control male cells, as well as a striking change in shape, shifting from disk-like shape (oblate) (**Figure 11L**) to an egg shape (prolate) (**Figure 11K**). We could also observe a decrease in Iba-1 intensity (**Figure 11J**), probably due to the increased volume occupied by the cells, that led to a dilution of the Iba-1 signal.

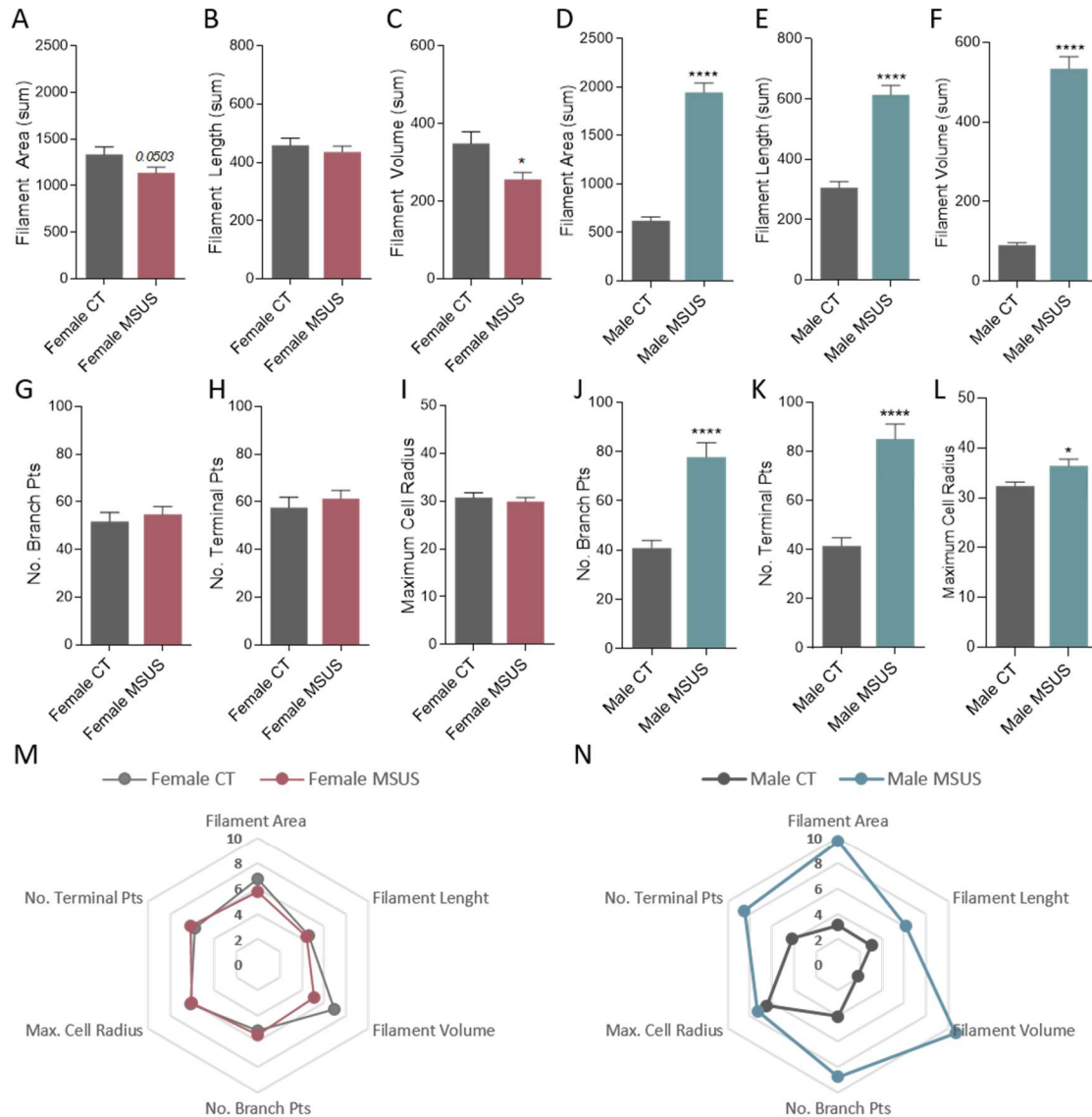


**Figure 10 – Filament analysis of microglia cells in the mPFC of P40 control and MSUS mice.** Microglia from P40 male and female control and MSUS animals were observed under a confocal microscope following Iba-1 immunohistochemistry. Z-stacks were collected of isolated cells in order to perform 3D reconstruction and filament analysis using the Imaris software. Several parameters were compared between the experimental groups, including **A** and **D**) filament area (expressed in µm²), **B** and **E**) filament length (expressed in µm), **C** and **F**) filament volume (expressed in µm³) **G** and **J**) number of branching points, **H** and **K**) number of ending points and **I** and **L**) maximum cell radius (expressed in µm). **M** and **N**) present radar plots for all parameters in the previous graphs. Results are representative of at least n=40 cells, 10 cells/animal for each experimental group. \*P ≤ 0.05, \*\*P ≤ 0.01, \*\*\*P ≤ 0.001, \*\*\*\*P ≤ 0.0001 with respect to control group, according to unpaired t-test with Welch's correction. Data are presented as mean ± SEM.

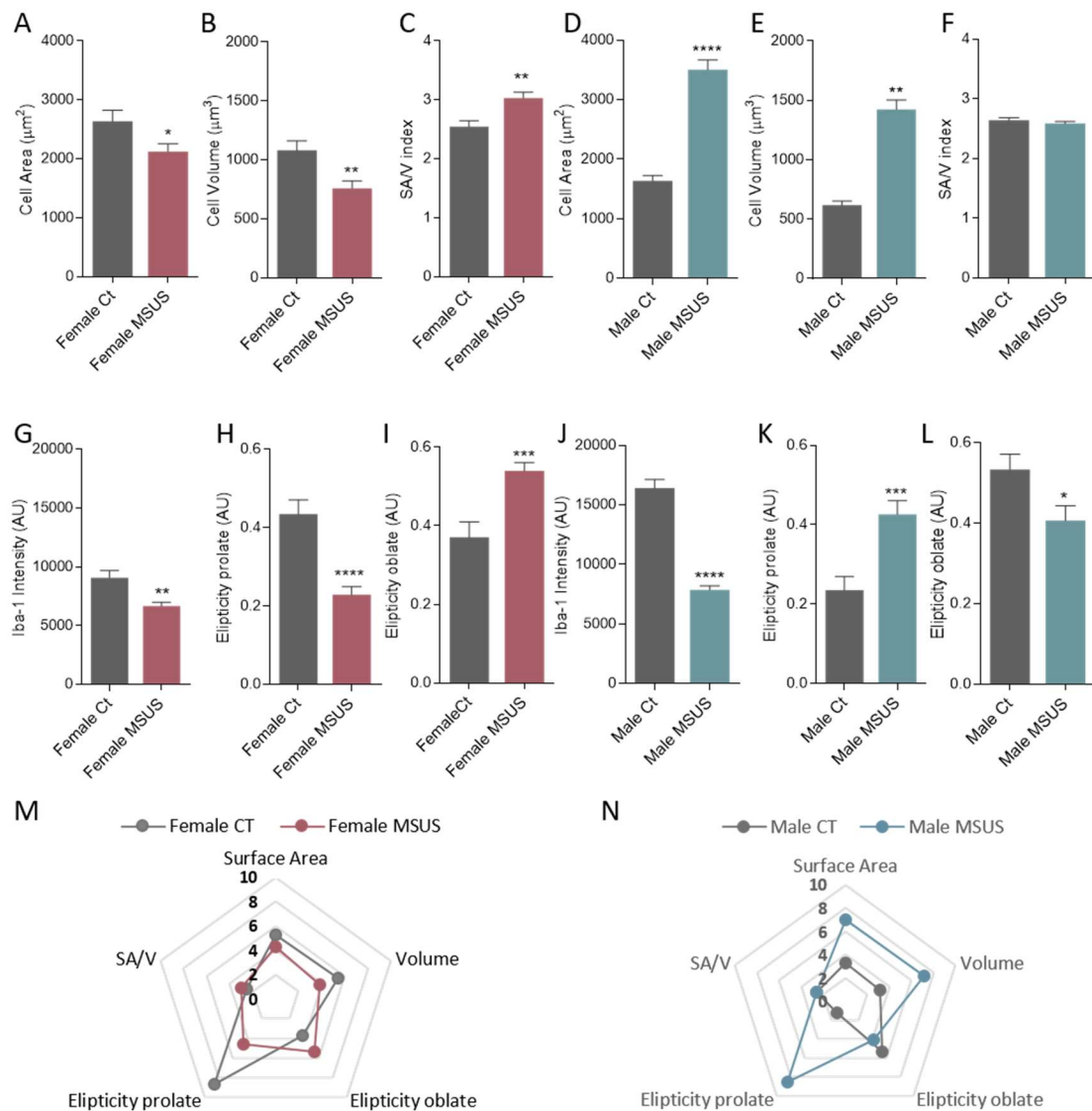


**Figure 11 – Surface analysis of microglia cells in the mPFC of P40 control and MSUS mice.** Microglia from P40 male and female control and MSUS animals were observed under a confocal microscope following Iba-1 immunohistochemistry. Z-stacks were collected of isolated cells in order to perform 3D reconstruction and filament analysis using the Imaris software. Several parameters were compared between the experimental groups, including **A** and **D**) total cell area (expressed in  $\mu\text{m}^2$ ), **B** and **E**) total cell volume (expressed in  $\mu\text{m}^3$ ), **C** and **F**) surface area/volume, **G** and **J**) Iba-1 intensity, **H** and **K**) ellipticity prolata and **I** and **L**) ellipticity oblate. **M** and **N**) present radar plots for all parameters in the previous graphs. Results are representative of at least  $n=40$  cells, 10 cells/animal for each experimental group. \* $P \leq 0.05$ , \*\* $P \leq 0.01$ , \*\*\* $P \leq 0.001$ , \*\*\*\* $P \leq 0.0001$  with respect to control group, according to unpaired t-test with Welch's correction. Data are presented as mean  $\pm$  SEM.

In contrast, at this age, MSUS females do not present significant changes in filament analysis, with respect to controls, with the exception of a small decrease in filament area and volume (**Figure 10A** and **10C**). However, we could observe significant changes in the overall cell surface that go in the opposite direction of those found in MSUS males, including a decrease in total area and volume (**Figure 11A** and **11B**, respectively), as well as a slight decrease in Iba1-intensity (**Figure 11G**) and a change in cell shape that was the opposite of that observed in males (**Figure 11H** and **11I**). These results point towards a higher susceptibility of MSUS male microglia to the long-term effects of ELS and suggest that an earlier adaptation of female microglia, during the acute period of stress, may prevent more drastic changes in microglia phenotype at a later time point.

In addition to the observed changes in microglia number and morphology, we also investigated if exposure to the MSUS protocol influenced microglia basic functions during the post-natal period, including the engulfment and elimination of entire neurons, which is actively taking place during the first week of the MSUS protocol (P2-P10), or the clearance of neuronal components, which has been associated with synaptic pruning and has been shown to occur throughout life, particularly during periods of intense synaptic remodelling.

Microglia clearance activity has been directly related with lysosome content. Therefore, in this study, we performed surface analysis following immunohistochemistry against CD68, a well described marker of lysosomes that is specific for immune cells, to detect changes in the volume and n<sup>o</sup> of CD68<sup>+</sup> particles inside control and MSUS microglia, both during the MSUS period (P10) and after the onset of puberty (P40) (**Figure 12**). While we did not observe any changes in the total number of CD68 particles/cell, either at P10 or at P40 (**Figure 12B** and **12F**), we were able to detect a reduction in the CD68/Iba-1 volume ratio in MSUS males (**Figure 12A**) at P10 and an increase in this parameter at P40 (**Figure 12E**). Since we did not find significant differences in cell volume in males at this age, we can conclude that this result is due to differences in CD68 total volume/cell. In fact, when we plotted this parameter (**Figure 12C**), we were able to detect two populations of cells in control males, one with a low total volume of CD68/cell and another with a high CD68 volume/cell, while in MSUS mice only one population of cells was observed, displaying low CD68 volume/cell. Since there were no significant differences in the number of particles per cell (**Figure 12B**), it stands to reason that a fraction of microglia in control male mice present CD68 particles with very large sizes, which is suggestive of a high clearance activity. The fact that MSUS male mice do not display these cells may indicate that their clearance activity is somewhat reduced. The reduction in total CD68 volume was also observed, to a lower extent, in female MSUS mice. At P40, the results observed in male MSUS mice go in the opposite direction, depicting an increase in CD68/Iba-1 ration in MSUS microglia (**Figure 12E**), but, once again, no changes in the total number of CD68 particles/cell (**Figure 12F**).

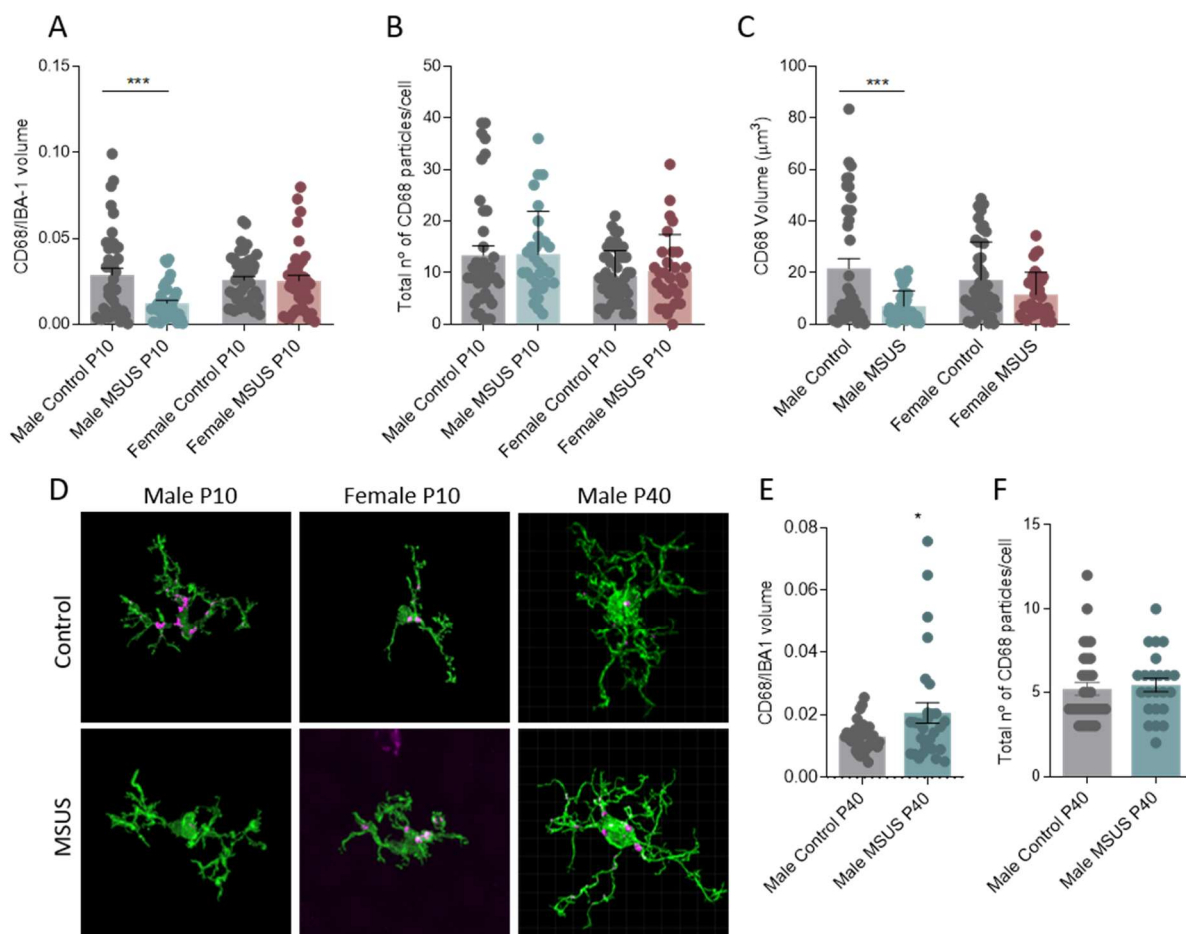


**Figure 12 – Surface analysis of CD68 positive particle in microglia cells in the mPFC of P10 and P40 control and MSUS mice.** Microglia from P10 male and female animals and P40 male animals were observed under a confocal microscope following Iba-1 and CD68 immunohistochemistry. Z-stacks were collected of isolated cells in order to perform 3D reconstruction and surface analysis using the Imaris software. Several parameters were compared between the P10 experimental groups, including **A**) CD68/Iba-1 volume, **B**) total n<sup>o</sup> of CD68 particles/cell and **C**) total CD68 volume/cell (expressed in μm<sup>3</sup>). A similar analysis was performed at P40 in male MSUS animals, including **E**) CD68/Iba-1 volume and **F**) total n<sup>o</sup> of CD68 particles/cell. **E**) displays representative images of control and MSUS microglia, showing Iba-1 staining in green and CD68 staining in purple. Results are representative of at least n=30 cells, 10 cells/animal for each experimental group. \*P ≤ 0.05 and \*\*\*P ≤ 0.001 with respect to the sex-matched control group, according to unpaired t-test with Welch's correction. Data are presented as mean ± SEM.

Taking into consideration the changes in morphology and CD68 content observed in male MSUS males, we next investigated the gene expression profile of P10 and P40 microglia in order to understand if these changes could be related to a higher expression of pro-inflammatory markers, which have been associated with a decrease in phagocytosis activity (**Figure 13**). qRT-PCR results showed that, in agreement to our hypothesis, P10 male MSUS mice presented an increase in the levels of pro-inflammatory markers IL-1 $\beta$  (**Figure 13A**) and IL-6 (**Figure 13B**) and a very expressive decrease in the levels of anti-inflammatory cytokine IL-10 (**Figure 13D**). These results correlate with the morphological changes observed at this age and corroborate the proposed shift of MSUS microglia towards a M1-like phenotype during the acute phase of stress. This shift seems to be at least partially irreversible, since a decrease in M2 marker Arg could still be found at P40, although the increase in pro-inflammatory markers is no longer visible.

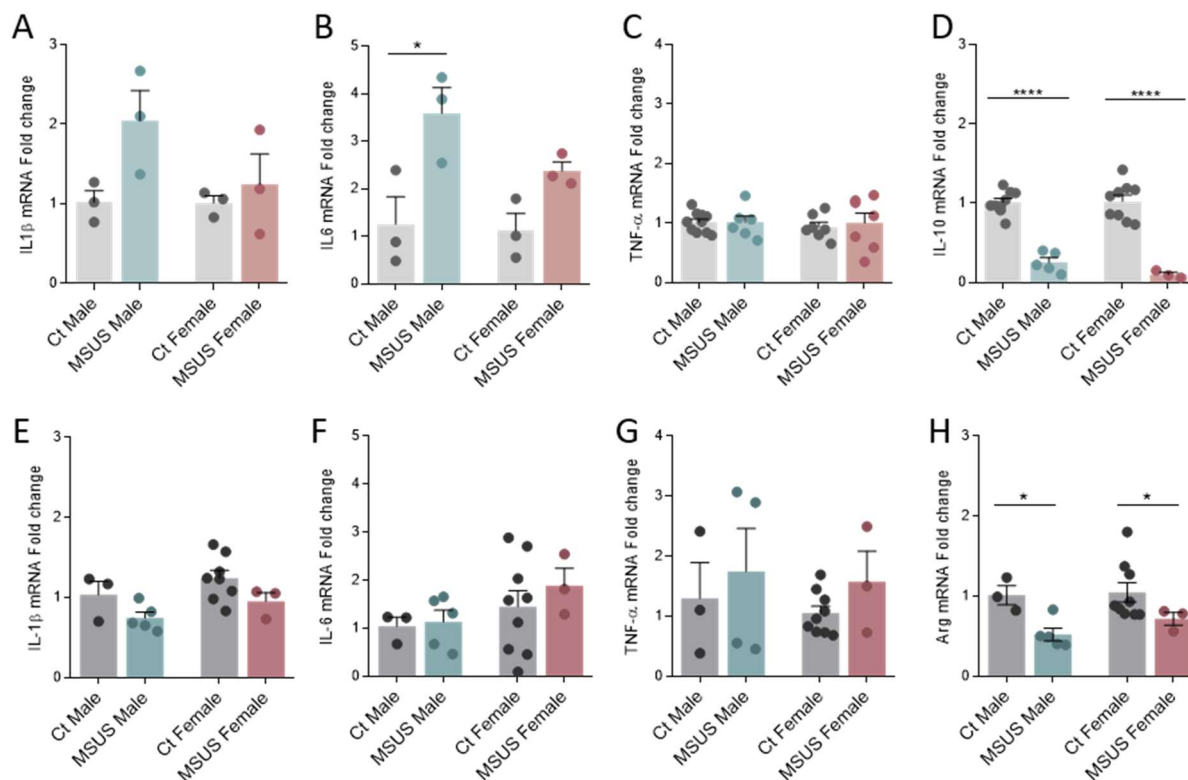


**Figure 15 – mPFC expression levels of pro- and anti-inflammatory genes at P10 and P40.** RNA samples were collected from the mPFC of MSUS and control male and female mice at P10 (A, B, C and D) and P40 (E, F, G and H) and the relative mRNA levels of **A** and **E**) IL-1 $\beta$ , **B** and **F**) IL-6, **C** and **G**) Tnf- $\alpha$ , **D**) IL-10 and **H**) Arg were determined by qRT-PCR. Results are expressed as fold change with respect to male controls and are representative at least n=5 for MSUS animals and n=9 for controls. \*P  $\leq$  0.05 and \*\*\*\*P  $\leq$  0.0001 between MSUS animals and sex-matched controls, according to unpaired t-test with Welch's correction. Data are presented as mean  $\pm$  SEM.

We next focused our attention on understanding the functional consequences of the morphological and gene expression changes detected in microglia cells upon exposure to ELS. We specifically explored microglia contribution to the elimination of inhibitory neurons, which is programmed to occur in the mPFC between P5-P10. These neurons are crucial for the regulation of the excitatory inputs that leave the mPFC towards other brain regions. Consistently with this function, inhibitory neuronal activity in the mPFC is directly involved in cognition and impulse control and alterations in these neurons have been shown to contribute to disturbances in oscillatory network synchrony and E/I balance that are thought to underlie cognitive deficits in schizophrenia and other mental illnesses<sup>13</sup>.

Inhibitory neurons in the mPFC can be divided in two main categories, parvalbumin (PV) positive fast spiking neurons (majority of inhibitory neurons in the mPFC) and somatostatin neurons. Parvalbumin is a calcium binding protein, whose expression (starting around P12 in the mPFC) coincides with the full maturation of the cortical circuits and the onset of  $\gamma$ -oscillations. PV<sup>+</sup> fast-spiking neurons can be further divided in basket and chandelier cells, which have different axonal morphologies and a slightly different distribution in mPFC cortical layers. While basket cells target the pyramidal cell body and proximal dendrites and can be found throughout layers 2-6, chandelier cells display vertical arrays of synaptic boutons (cartridges) that enervate the proximal

segment of the pyramidal neuron axon and appear only in the border of layers 1/2<sup>13</sup>. The maturation of the fast-spiking phenotype PV<sup>+</sup> neurons is finished by the onset of puberty and is highly dependent on the excitatory input from pyramidal neurons, which makes them particularly susceptible to changes in excitatory drive during the first 4 weeks of life.

In this work we employed a knock-in mouse model currently available at CNC, the PV-tdTomato animals, which express the red fluorescent protein tdTomato under the control of the parvalbumin (PV) promoter, thus presenting fluorescent labelling in PV<sup>+</sup> inhibitory neurons throughout the brain, including in the mPFC. We performed stereology in P40 control and MSUS PV-tdTomato animals to estimate the number of these neurons in the different regions and layers of the mPFC.

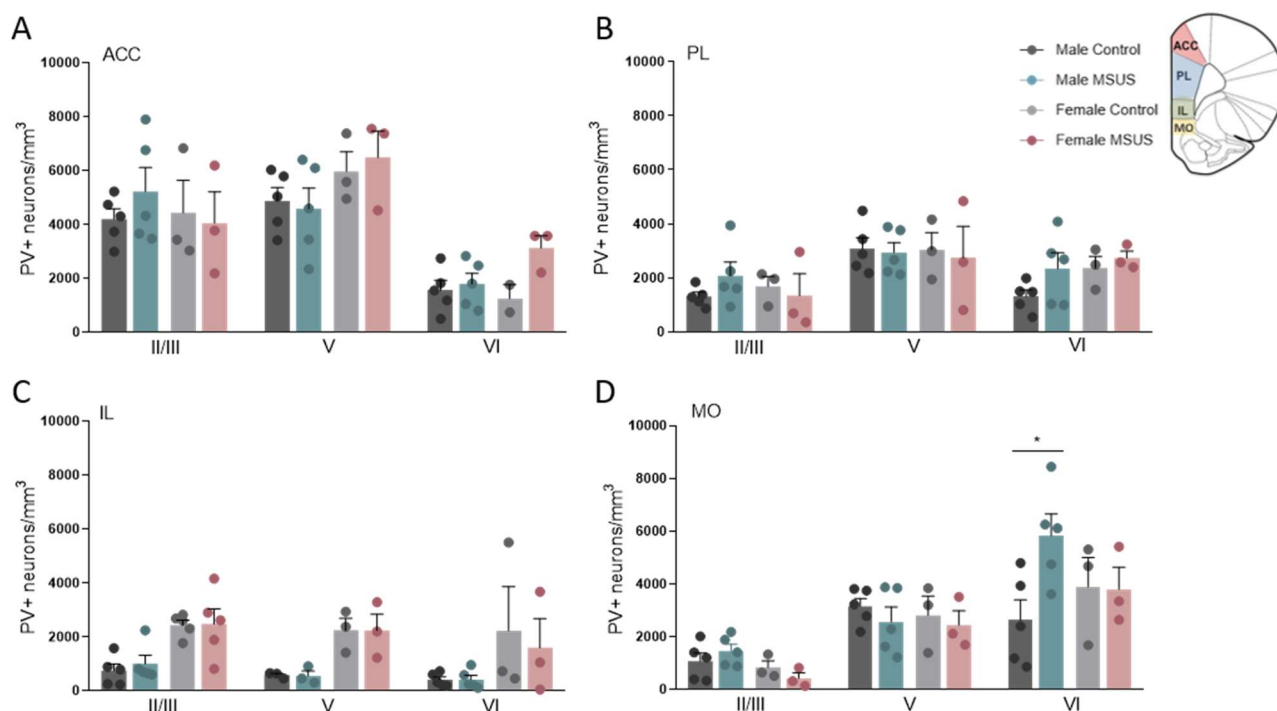


**Figure 14 – Stereology-based evaluation of total number of PV<sup>+</sup> neurons in the different subregions and layers of the mPFC.** The mPFC was divided in four sub-regions; anterior cingulate cortex (ACC), prelimbic region (PL), infralimbic region (IL) and medial orbital cortex (MO). The total number of PV<sup>+</sup> neurons in the total volume of each region was estimated by stereology, for each of the designated regions A) ACC B) PrL, C) IL and D) MO, using a Zeiss Z2 microscope and the StereoInvestigator software. Results are expressed as the number of cell/mm<sup>3</sup> and are representative of at n=5 for males and n=3 for females. \*P ≤ 0.05 and \*\*\*P ≤ 0.001 with respect to the sex-matched control group, according to unpaired t-test with Welch's correction. Data are presented as mean ± SEM.

Ours results clearly show the expected distribution of PV<sup>+</sup> neurons across the different cortical layers present in the mPFC (Figure 14). It is clear that these neurons are more frequent in the anterior cingulate cortex (Figure 14A) and prelimbic regions (Figure 14B) and less frequent in the infralimbic region (Figure 14C). In addition, the infralimbic region presented an interesting sexual dysmorphic patten, exhibiting a higher number of PV<sup>+</sup> neurons in females than in males (Figure 14C).

Exposure to the MSUS protocol led to a significant and specific increase in the number of PV<sup>+</sup> neurons in the medial orbital cortex in male animals (Figure 14D), and a similar tendency in the prelimbic cortex (Figure 14B). These differences were observed specifically in layer VI, where we can find the excitatory pyramidal neurons that project towards the limbic regions and that are responsible, for example, for the control exerted by the mPFC over other regions during stress response, such as the amygdala. The observed increase in the number of PV<sup>+</sup> neurons in layer VI, together with the increase in spontaneous inhibitory activity detected in the mPFC of adult male MSUS males, led us to hypothesize that ELS exposure triggers and increase in the inhibitory tonus received by layer VI projection neurons, which could limit the influence of the mPFC during stress response and potentiate the impulsive behaviors and changes in social hierarchy observed in male MSUS animals.

PV<sup>+</sup> neurons originate mainly in the medial ganglionic eminence (MGE), migrating first tangentially to the cortical plate and then radially to reach their final destinations within the cortical layers. This process begins during the embryonic period and is usually finished by P10. Nevertheless, in order to discard the hypothesis that the observed increase in the number of PV<sup>+</sup> neurons was due to changes in the migration pattern of these neurons,

and since PV expression in the mPFC only starts around day 12, we looked for the expression levels of genes implicated in the migration and placement of inhibitory neurons, including *Dlx2* (marker of inhibitory neurons arising in the MGE) and *erbb4* (specific for PV<sup>+</sup> neurons) (**Figure 15A** and **15B**), as well as to overall markers of GABA release (*VGAT*) and production (*GAD-1*) (**Figure 15C** and **15D**). We did not observe any significant differences in the expression of these genes at P10, which indicates that ELS exposure does not trigger significant changes in neuronal migration or distribution and does not impact the overall levels of inhibitory neurons in the mPFC. We further confirmed these results by looking to *GAD67* immunolabelling in the mPFC (data not shown), which did not reveal gross differences in the number or distribution pattern of inhibitory neurons.

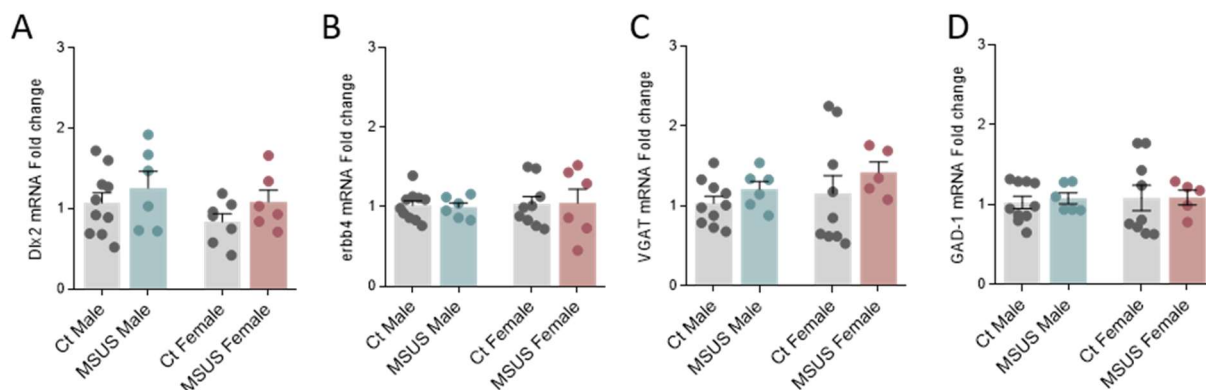


**Figure 15 – mPFC expression levels of genes implicated in inhibitory neuron migration and function at P10.** RNA samples were collected from the mPFC of MSUS and control male and female mice at P10 and the relative mRNA levels of A) *Dlx2*, B) *Erbb4*, C) *VGAT* and D) *GAD-1* were determined by qRT-PCR. Results are expressed as fold change with respect to male controls and are representative at least n=5 for MSUS animals and n=9 for controls. No significant differences were found between MSUS animals and sex-matched controls, according to unpaired t-test with Welch’s correction. Data are presented as mean ± SEM.

## 5. CONCLUSIONS AND FUTURE PERSPECTIVES:

The work performed during the three years of this project allowed us to characterize some of the behavioral changes that emerge in juvenile and adolescent rodents upon exposure to an early life stress paradigm that mimics maternal stress and neglect. The maternal separation and unpredictable stress (MSUS) protocol employed in this study was sufficient to induce changes in maternal behavior that led to a decrease in pup weight and to changes in the number and profile of ultravocalizations in both male and female juvenile mice, suggesting that a reduction in caring behavior can lead to a weaker maternal bond that impacts pup development and social skills from an early age. However, although we observed similar changes in male and female mice exposed to MSUS during the acute stress period, long term effects in behavior were only observed in male animals. Throughout our study, female adolescent MSUS mice were significantly more resilient to the effects of stress, not showing any behaviour differences compared to their age-matched controls, while we could identify a decrease in social preference and an increase in risk-taking and depressive-like behaviour in adolescent male mice. These findings are in accordance with previous works showing a stronger impact of ELS exposure in male animals and with previous work from our group, also in the scope of this grant, where we showed changes in social memory and social hierarchy in adult MSUS male mice (see Franco et al, under revision).

The first two weeks of life correspond to a period in which microglia cells are known to play crucial roles in the correct wiring of neuronal circuits. These roles include the elimination of neuronal precursors and synaptic pruning, thus allowing the strengthening of synapses that accompanies the maturation of neuronal connections. In this project, we have performed an extensive morphologic and phenotypic characterization of microglia in both control and MSUS mice, as well as an assessment of microglia contribution to the establishment of mPFC inhibitory networks, paying special attention to sex-driven molecular/cellular changes that can explain differential behavior outcomes.

Overall, our results strongly suggest that exposure to early life stress interferes with microglia functions during the post-natal period by inducing changes in microglia morphology, phagocytic capacity and gene expression that remain until after puberty onset. Furthermore, our data points towards the existence of important sexual dimorphisms in microglia cells, both under control and ELS conditions. The higher stress resilience observed in females may be related with the different adaptive responses observed in female and male microglia, both

during the acute period of stress and at later time points. Although both male and female microglia displayed similar changes in gene expression during the juvenile and adolescence periods, MSUS males presented a significant decrease in CD68 content at P10, indicating a reduction in microglia-mediated phagocytic activity during a critical period for neuronal elimination. In addition, male but not female MSUS microglia showed a reduction in the number of ramifications and cell volume, as well as an increase in Iba-1 intensity that is compatible with a shift towards a pro-inflammatory M1-like activation phenotype, which has been suggested to disrupt homeostatic microglia functions. Female microglia cells presented the opposite morphological response during the acute period of stress, showing hyper-ramification. Interestingly, while the changes in female MSUS microglia diluted with time, and control and MSUS female cells became indistinguishable at P40, microglia from MSUS males showed even more dramatic morphologic changes at P40, presenting a hyper-ramified phenotype and surface parameters that resemble those of age-matched female microglia.

Our current hypothesis is that these changes might prevent the correct engulfment of inhibitory neuronal precursors during one of the critical periods of mPFC circuit maturation. In this context, we observed an increase in the number of PV<sup>+</sup> neurons specifically in layer VI of the medial orbital and prelimbic cortexes in male tdTomato MSUS mice. We believe that a higher number of inhibitory interneurons in this layer may cause long term impairments in internal mPFC circuitry, compromising long-range connectivity between the mPFC and ventral limbic structures, which might help explain the overall behaviour changes observed in MSUS males, both during the adolescent period and in adulthood. Female MSUS animals did not present significant changes in the number of PV<sup>+</sup> neurons, as well as no overt changes in behaviour, which further supports this hypothesis.

Overall, we believe this work provides critical evidence of relevant sexual dimorphic features in the mouse brain, including at the neuroimmune level, that support the different responses males and females present to ELS. These results further stress the need to continue exploring the moderating effects of sex on psychopathologies.

## 6. BIBLIOGRAPHY:

1. Arango, C. *et al.* Preventive strategies for mental health. *Lancet Psychiatry* **5**, 591–604 (2018).
2. White, J. D. & Kaffman, A. Editorial Perspective: Childhood maltreatment – the problematic unisex assumption. *J Child Psychol Psyc* (2019) doi:10.1111/jcpp.13177.
3. Beery, A. K. & Zucker, I. Sex bias in neuroscience and biomedical research. *Neurosci Biobehav Rev* **35**, 565–572 (2011).
4. Wong, F. *et al.* Pyramidal cell regulation of interneuron survival sculpts cortical networks. *Nature* **557**, 668–673 (2018).
5. Grabert, K. *et al.* Microglial brain region–dependent diversity and selective regional sensitivities to aging. *Nat Neurosci* **19**, 504–516 (2016).
6. Salter, M. W. & Stevens, B. Microglia emerge as central players in brain disease. *Nat Med* **23**, 1018–1027 (2017).
7. Wlodarczyk, A. *et al.* A novel microglial subset plays a key role in myelinogenesis in developing brain. *Embo J* **36**, 3292–3308 (2017).
8. Hagemeyer, N. *et al.* Microglia contribute to normal myelinogenesis and to oligodendrocyte progenitor maintenance during adulthood. *Acta Neuropathol* **134**, 441–458 (2017).
9. Sierra, A., Gottfried-Blackmore, A., Milner, T. A., McEwen, B. S. & Bulloch, K. Steroid hormone receptor

expression and function in microglia. *Glia* **56**, 659–674 (2008).

10. Bicks, L. K., Koike, H., Akbarian, S. & Morishita, H. Prefrontal Cortex and Social Cognition in Mouse and Man. *Front Psychol* **6**, 1805 (2015).

11. Xu, P., Chen, A., Li, Y., Xing, X. & Lu, H. Medial prefrontal cortex in neurological diseases. *Physiol Genomics* **51**, 432–442 (2019).

12. del Pino, I., Rico, B. & Marín, O. Neural circuit dysfunction in mouse models of neurodevelopmental disorders. *Curr Opin Neurobiol* **48**, 174–182 (2018).

13. Miyamae, T., Chen, K., Lewis, D. A. & Gonzalez-Burgos, G. Distinct Physiological Maturation of Parvalbumin-Positive Neuron Subtypes in Mouse Prefrontal Cortex. *J Neurosci* **37**, 4883–4902 (2017).